GEOPHYSICS, VOL. 84, NO. 1 (JANUARY-FEBRUARY 2019); P. E13–E22, 11 FIGS., 1 TABLE.
10.1190/GEO2018-0355.1

tTEM — A towed transient electromagnetic system for detailed 3D imaging of the top 70 m of the subsurface

Esben Auken[1], Nikolaj Foged[1], Jakob Juul Larsen[2], Knud Valdemar Trøllund Lassen[3], Pradip Kumar Maurya[1], Søren Møller Dath[1], and Tore Tolstrup Eiskjær[1]

ABSTRACT

There is a growing need for detailed investigation of the top 30–50 m of the subsurface, which is critical for infrastructure, water supply, aquifer storage and recovery, farming, waste deposits, and construction. Existing geophysical methods are capable of imaging this zone; however, they have limited efficiency when it comes to creating full 3D images with high resolution over dozens to hundreds of hectares. We have developed a new and highly efficient towed transient electromagnetic (tTEM) system, which is capable of imaging the subsurface up to depth of 70 m at a high resolution, horizontally and vertically. Towed by an all-terrain vehicle, the system uses a 2×4 m transmitter coil and has a z-component receiver placed at 9 m offset from the transmitter. The tTEM uses dual transmitter moment (low and high moment) measurement sequence to obtain the early and late time gates corresponding to shallow and deep information about the subsurface layers. The first bias-free gate is as early as 4 μs from beginning of the ramp (1.4 μs after end of ramp). Data are processed and inverted using methods directly adopted from airborne electromagnetics. The system has been successfully used in Denmark for various purposes, e.g., mapping raw materials, investigating contaminated sites, and assessing aquifer vulnerability. We have also used the tTEM system in the Central Valley of California (United States) for locating artificial recharge sites and in the Mississippi Delta region, to map complex subsurface geology in great detail for building hydrogeologic models.

INTRODUCTION

This paper presents a newly developed, towed, ground-based transient electromagnetic (tTEM) system, designed for highly efficient and detailed 3D geophysical and geologic mapping of the shallow subsurface. Detailed 3D geophysical/geologic information in this near-surface zone is demanded in many cases, e.g., estimation of groundwater vulnerability to contamination (Ibe et al., 2001; Focazio, 2002) and possible regulation of land use (Mayer and Somerville, 2000), infrastructure development (Look, 2014), artificial infiltration cases (Bouwer, 2002), surface and groundwater interaction in the near surface (Sophocleous, 2002), among others.

The tTEM system fills a gap in the geophysical toolbox, which lacks systems capable of efficiently providing resistivity information in the target depth range of 0–70 m. Although the systems capable of resolving features in this range do exist, they most often are limited in either resolution or mapping efficiency when a detailed coverage in full 3D is needed for survey areas larger than a few hectares. Electrical resistivity tomography (ERT), in the right configuration, can provide the needed resolution in the upper 50–70 m, but the data collection is relatively inefficient because the ground electrodes need to be moved for surveying larger areas. The ERT method (Loke et al., 2013; Binley, 2015) is therefore often used in profiling mode, providing 2D resistivity sections or with parallel 2D profiles for 3D resistivity mapping of smaller confined targets (Dahlin et al., 2002; Maurya et al., 2017). Towed or pulled direct current systems, such as the PACES-system (Sørensen, 1996; Christensen and Sørensen,

Manuscript received by the Editor 8 May 2018; revised manuscript received 24 July 2018; published ahead of production 03 October 2018; published online 28 November 2018.
[1]Aarhus University, HydroGeophysics Group, Department of Geoscience, Aarhus, Denmark. E-mail: esben.auken@geo.au.dk; nikolaj.foged@geo.au.dk; pradip.maurya@geo.au.dk; smd@geo.au.dk; tore.eiskjaer@geo.au.dk.
[2]Aarhus University, Department of Engineering, Aarhus, Denmark. E-mail: jjl@eng.au.dk.
[3]Formerly Aarhus University, HydroGeophysics Group, Department of Geoscience, Aarhus, Denmark; presently Aarhus Geosoftware Aps, Aarhus, Denmark. E-mail: kvtl@aarhusgeosoftware.dk.

2001), and the Ohm-Mapper by Geometrics Inc. (Garman and Purcell, 2004), have a higher field efficiency and can therefore provide the needed lateral resolution by continuously measuring along densely spaced lines. The Ohm-Mapper uses capacitive coupling to the ground for current injection, but is limited to a surveying depth of approximately 8 m and an operation speed of 2–5 km/h (Garman and Purcell, 2004). The PACES system was used intensively in the 1990s, primarily for vulnerability mapping in the Danish national groundwater campaign (Møller et al., 2009). The PACES system has a higher operation speed (6–7 km/h), but despite a 100 m long electrode tail holding eight quadrupole configurations, the depth of investigation (DOI) is limited to 15–20 m.

Ground-conductivity meters (GCMs) have been used in many cases for covering relatively large areas with dense line spacing (usually 10–15 m) by towing the instrument with an all-terrain vehicle (ATV) or similar, e.g., in soil-mapping contexts. The newer GCM-instrument, e.g., DUALEM-421 by DUALEM Inc., has multiple receivers built into the same instrument tube and, therefore, can provide high-resolution 3D resistivity information of the shallow subsurface (Saey et al., 2015; Christiansen et al., 2016), but in a limited depth range (0–7 m).

For high data-collection efficiency and for surveying large areas, airborne electromagnetic (AEM) is preferred (Fitterman, 2015; Auken et al., 2017). Helicopter frequency-domain systems typically have a shallower focus depth compared with airborne TEM systems (ATEM), but ATEM systems such as SkyTEM (Sørensen and Auken, 2004) are constantly pushing the limit for detailed near-surface mapping. In particular, this is achieved by measuring more and more unbiased early time gates or by measuring the full system response (Andersen et al., 2015). Despite this, the ground-based methods (e.g., GCM, ERT) still have a superior resolution in the top 0–20 m compared with AEM. AEM systems also operate with line spacing of several hundreds of meters, thereby limiting the lateral resolution. Even if the line spacing is reduced, e.g., to 50 m (Schamper et al., 2014b), the larger footprint of the AEM systems compared with ground-based systems is still a limiting factor (Christensen, 2014) to achieve higher lateral resolution. Finally, AEM systems have a high mobilization cost, making them relatively expensive for surveying smaller areas.

Towed or pulled ground-based TEM is not a new idea. The pulled array TEM system (Sørensen, 1997) used in 1999–2001 in the Danish national groundwater campaign had other design goals than the tTEM system. Additionally, the TEM instrumentation at that time was unable to deliver unbiased early time gates (<10 μs) for very near-surface resolution. Today, some commercial TEM-instrument manufacturers offer towed ground-based or even floating TEM systems (e.g., Dynamic NanoTEM from Zonge; Harris et al., 2006), but a comprehensive system validation/mapping capability test of these systems, seems not to be available.

In this paper, we introduce the tTEM system reviewing the different design aspects, and we present a detailed validation of the system. We present mapping results from a 156 ha survey showing a high-resolution image of the subsurface with horizontal resolution down to 25 × 10 m.

THE tTEM SYSTEM

System descriptions

The design goal for tTEM system was to make a TEM system that provides a high lateral resolution (approximately 10 m) and a vertical resolution resolving layers from top 2–3 m and to a depth of at least approximately 40 m (within the resolution limits of any diffusive EM method). The actual system, however, turned out to have a 70 m investigation depth. Furthermore, we demanded an efficient data collection, so that areas of few hectares up to approximately 10 km^2 can be mapped in a reasonable time and at a reasonable cost.

Figure 1 shows the present layout of the tTEM system. The ATV carrying the instrumentation is towing the transmitter frame (Tx coil), with the receiver coil (Rx coil) at a 9 m offset (coil-to-coil center). The Tx and Rx coils are mounted on sleds for a smooth ride over rough fields. The operational speed of the tTEM system is 15–20 km/h. When surveying farmland, the sprayer tracks in the fields are often used as driving paths to minimize crop yield impact, resulting in a line spacing of approximately 20 m. Including mobilization and demobilization, and depending on field conditions, the production rate is approximately 1 km^2 per day (100 hectares per day). Navigation and data collection are monitored and controlled by the driver using a tablet PC. The tablet PC is a remote desktop display for the internal four-core i5-based PC, which runs the data acquisition and the navigation system. This navigation software is a full-scale geographical information system (GIS) interface displaying background GIS themes, survey paths and line numbers, status parameters, and various alarms from the system integrated with real-time GPS input. The geographical position of the data is recorded by two satellite-based augmentation system — GPS placed

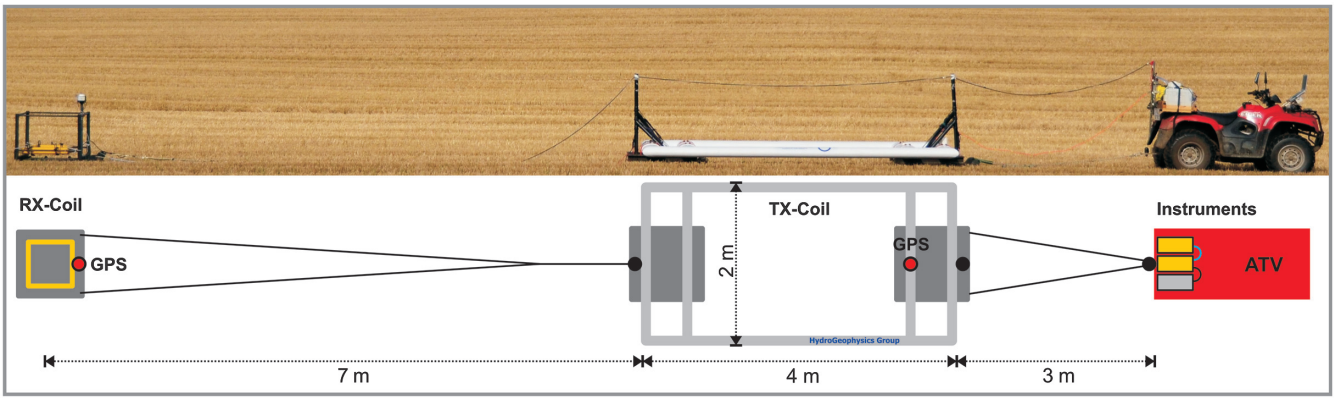

Figure 1. The tTEM system. Field photo from the side and top view layout of the system.

on the Tx-frame and on the Rx-sledge. The tTEM system can be operated by one person, but a second person is normally assigned to assist with the mobilization/demobilization, on-site survey planning, data quality control, and field safety.

The tTEM transmitter and receiver instrumentation are built using the same technology as the SkyTEM system (Sørensen and Auken, 2004) and WalkTEM system (Nyboe et al., 2010), but they are customized to achieve the tTEM design goals. The tTEM system uses a dual-transmitter moment measurement sequence to obtain the early and late time TEM data. A transient is measured after each transmitter pulse. The Rx coil is a 0.56×0.56 m multiturn coil with an area of 5 m^2, suspended induction coil measuring the vertical component. The cut-off frequency of the Rx coil is 670 kHz. Detailed system specifications are listed in Table 1. Based on a travel speed of 20 km/h and the pulse time in Table 1, the system moves approximately 3.3 m (0.6 s) during the raw stacking of the 422 LM and 264 HM transients. Down sampling this to a sounding for each 10 m yields approximately 1758 LM and 1122 HM transients in an averaged stack used for inversion.

Design aspects

Configuration

For operational efficiency, the Tx coil must be relatively small for a towed TEM system, which resulted in the 2×4 m dimension of the tTEM Tx coil/frame. A small Tx frame size is convenient to drag over fields and also when moving between fields without disassembling. The 2×4 m frame also fits on a car trailer, making the tTEM system easy to mobilize. Additionally, it can easily be disassembled and shipped.

A central loop configuration is commonly used for ground-based TEM, in which the Tx coil, is 40×40 m or bigger. Placing the Rx coil in the center of a small Tx coil (close to the Tx-wire), gives a strong coupling between the Tx and Rx coil, and it results in a huge primary magnetic field, saturating the amplifiers in the receiver system. This makes recording of unbiased early time gates (<10 μs) containing the very near-surface information, difficult or impossible. For ATEM systems, the strong coupling between the Tx and Rx coils is reduced by placing the Rx coil in a zero position (Schamper et al., 2014a) or using a central loop configuration with a bucking coil, or using an offset configuration (Auken et al., 2015). For the tTEM system, an offset configuration was chosen to be the best solution in terms of minimizing capacitive coupling between the Rx system and the Tx system and avoiding amplifier saturation with an otherwise unavoidable harmonic distortion.

Depth of investigation

The DOI (Christiansen and Auken, 2012) is related to the signal-to-noise ratio (S/N), which is proportional to $I_{Tx} * A_{Tx} * \sqrt{N}$, where I_{Tx} is the Tx-current, A_{Tx} is the Tx-area, and N is the number of transients in the average stack. The relatively small Tx coil area (8 m^2) therefore poses a challenge to obtain a sufficient DOI. To increase the transmitter moment, we used high Tx-current (30 A) for HM data, resulting in an HM peak moment of 240 Am^2. Furthermore, we record the TEM signal with a high pulse-repetition frequency (see Table 1), which enables us to cancel out random noise in raw stacks. During the post data processing, adjacent raw stacks are further averaged over a distance (typically 10 m) and thereby increase the S/N and the DOI. With this setup, a DOI of 60–70 m is obtained in an average resistivity environment of 40–60 Ωm, considerably deeper than our design goal of 40 m.

Tx-temperature and current control

The current diffusion into the ground for TEM is fast, so the key to obtaining very near surface resolution with a TEM-system is a fast turn-off and immediate recording of an unbiased signal. The turn-off time depends primarily on I_{Tx}, the capacitance and self-inductance of the Tx-loop, and the loop damping. With a 200 Ω damping resistor in parallel, the system turns off the approximately 3 A LM-current in approximately 2.5 μs and has the first unbiased time gate after just 1–2 μs from end of the turn-off.

To prevent overheating in the transmitter due to the very high repetition frequency and high transmitter current, the transmitter unit is water cooled. The fluctuating Tx temperature has a significant impact on the magnitude of the transmitted current. This is clearly seen in Figure 2a, in which we observe a linear relationship between the temperature, measured directly on the mosfet transistors on the Tx board, and HM transmitted current. A fluctuating transmitter current again impacts the turn-off time/the shape of the transmitter waveform, as shown in Figure 2b, in which the LM turn-off waveforms at different temperatures, measured with a small (>1 MHz resonance frequency) induction coil placed next to the transmitter wire, are plotted. Integrating the induction coil responses from Figure 2b, one obtains the turn-off waveform as a function of current, as shown in Figure 2c.

In the modeling of tTEM data, it is important to accurately model the shape of the waveform to avoid a significant bias in the modeling (Bedrosian et al., 2015). This is not as important for late time gates, but it is crucial for the early gates in which the first gate opens approximately 1 μs from end of ramp. Because it is impossible to measure the waveform continuously, we use a fixed waveform for

Table 1. System specification with the separate entries for the low-moment (LM) and high-moment (HM) configurations.

	Low moment (LM)	High moment (HM)
Transmitter area (single turn)	8 m^2	8 m^2
Tx current	~2.8 A	~30 A
Tx peak moment	~22.4 Am^2	~240 Am^2
Pulse repetition frequency (50 Hz power line frequency)	2110 Hz	660 Hz
Number of pulses/time	422/0.20 s	264/0.40 s
Duty cycle	42%	30%
Tx on-time	200 μs	450 μs
Turn-off time	2.5 μs	4.0 μs
Gate time interval (from beginning of turn-off)	4–33 μs	10–900 μs
Number of gates	15	23

the Tx. To do so, we regulate the transmitter cooling, enabling us to keep the instrument temperature within ±2° of the target operating temperature 45° and we regulate the input voltage to keep a constant current with fluctuations less than 3%. Fluctuations in the transmitter current itself do not introduce a data-level error because the current is measured for each raw stack, and data are normalized with this current. However, changing the magnitude of the current changes the shape of the waveform. The waveform in Figure 2c is discretized piecewise linearly in 20 pieces and modeled in the forward code. The turn-off time in Table 1 is defined as the time when the I_{Tx} is decreased to 0.5% of the maximum amplitude.

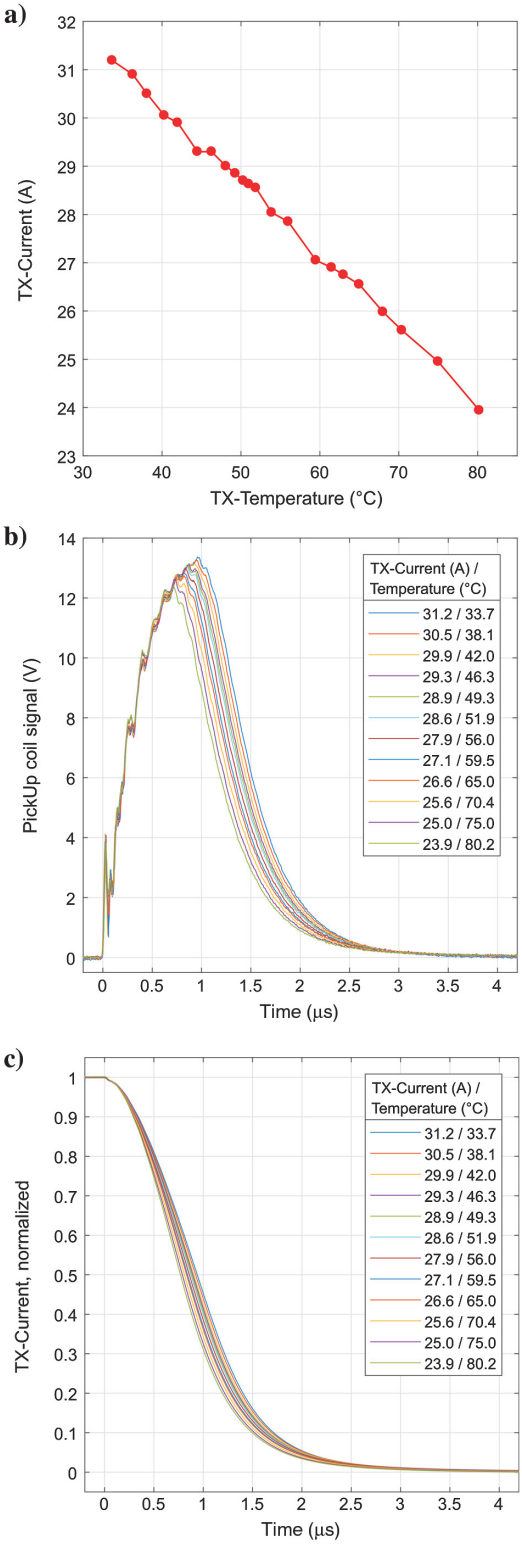

Figure 2. (a) Tx-current versus Tx-temperature for HM, (b) LM waveform at varying current/temperature, and (c) LM turn-off ramp at varying currents/temperatures scaled to unity current.

Device locations

TEM instruments are in general very sensitive instruments, and one can easily introduce noise/bias in the data due to coupling to conductive objects placed near the instrumentation, Tx, and/or Rx coil. For this reason, the Tx-frame and Tx and Rx sleds are constructed of nonconductive components (composite material, wood, and plastic) to avoid any extraneous signals. The instrumentation, cabling, GPS receivers, ATV, and other nearby conducting objects, however, are all potential noise/coupling sources.

For ATEM systems, it is relatively easy to check and quantify the internal system noise/bias response level by taking the system to a high altitude (greater than 1000 m), where the secondary EM response from the earth is negligible. For the tTEM system, it is not practical to perform such a high-altitude test, especially when including the full system with an ATV. Instead, numerous tests were performed on a resistive site (>600 Ωm in the upper approximately 120 m), in which the earth response was relatively low, thereby enabling us to spot potential bias signals and their sources. The tTEM system layout has primarily been decided based on these test measurements, ensuring that any bias signal introduced by the system components is smaller than 1% of the measured earth signal.

We investigated the effect of the ATV on the signal recorded at the same resistive test site, at multiple distances from the front of the Tx-frame. Figure 3 shows an example of a data section. Figure 3a shows the single HM gate values with the ATV separated 1, 2, 3, and 4 m from the front of the Tx coil. Figure 3b shows the center HM sounding curves of the four ATV distances.

It is clearly seen in Figure 3a and 3b that the signal level is higher at the late time gates with an ATV separation of only 1 and 2 m compared with the 3 and 4 m separations. Because the earth response is constant, the increased signal at 1 and 2 m is a coupling response from the ATV, so the Tx induces a current in the ATV, which then decays and is added to the earth signal measured in the Rx coil. At an ATV distance of 3 and 4 m (and greater), we get coincident responses within the data uncertainty. From this test, we can conclude that a safe ATV distance to the Tx coil is 3 m. Similar tests have been conducted for Tx-Rx offset distance and all other measurement system components to make sure that no significant bias signal is introduced in the data.

Using an offset configuration and a nonfixed Rx-Tx geometry poses some modeling challenges regarding the system geometry. Pitch and roll of a few degrees of the Tx-Rx coils gives changes to the signal level of much less than 1% (Kirkegaard et al., 2012) and can be neglected. For a central loop configuration with large transmitter loops, one can displace the receiver coil from the center position by several meters without having a significant impact on the measured secondary response. However, an offset system is considerably more sensitive to the transmitter-receiver geometry. Figure 4 shows the modeling error for the LM time gates of the tTEM system for different offsets from the nominal Tx-Rx offset

of 11 m. Figure 4 is compiled by calculating forward response for different Tx-Rx offsets for a 30 Ωm half-space and then calculating the percentage error relative to the nominal Tx-Rx offset. Figure 4 shows that the modeling error increases for earlier time gates and with increasing Tx-Rx offset. The modeling error also increases with decreasing half-space resistivity (not shown).

If an acceptable modeling error level is chosen to be 2%–3% (corresponding to the assigned data uncertainty for the early time gates), we then need, in the worst case, to be able to determine the Rx-Tx distance with a precision of approximately 20 cm or better. This precision can be obtained by using the Rx and Tx GPS-positions together. For survey areas with a top layer of higher resistivity than 30 Ωm, assuming a fixed Tx-Rx distance for the whole survey is justified as the towing rope is pulled tight during surveying and sideways moment of the Rx coil have a relatively small impact on the Tx-Rx distance (results are not shown here).

System validation at Danish National TEM test site

The final calibration and validation of the tTEM system was performed at the Danish national TEM test site (Foged et al., 2013), in which a well-documented resistivity model has been established by a 700 m long resistivity profile based on ground-based TEM soundings. The calibration/validation follows the procedure described by Foged et al. (2013), where a system-specific forward response (the reference response) is calculated for the resistivity model of the test site and compared with the recorded sounding curve at the test site. In the procedure of calibration, the necessary adjustment in the voltage data level is done by a factor called the calibration factor, and timing of the gates by a constant time shift. Figure 5 shows the reference response and a tTEM sounding from the test site after the final calibration. As seen in Figure 5, we obtain a good match to the reference response, well within the data error bars of approximately 3%. As an important note, the test-site validation is also a validation of the processing and modeling schemes used for the tTEM system.

The TEM test site also holds an approximately 700 m long reference line with 40 m spaced resistivity models, carried out as 40 × 40 m central-loop ground-based TEM soundings. The vertical resistivity column in Figure 6 is the reference models, and the continuous resistivity section is a smooth model inversion of the tTEM data. As expected, we obtain a very good overall match to the reference model section (Figure 6c). Figure 6a shows the data misfit of a representative sounding at 330 m (see the arrow in Figure 6c), and the corresponding resistivity model is shown in Figure 6b, together with the reference model. The quality of misfit for each sounding is calculated using the following formula which we refer to as the data residual d:

$$d = \sqrt{\frac{1}{N}\sum_{i=1}^{N}\frac{(\log(d_{\mathrm{obs},i}) - \log(d_{\mathrm{fwd},i}))2}{\sigma_{di}^2}}, \qquad (1)$$

where d_{obs} is the observed data, d_{fwd} is the forward data, σ_d is the error in the observed data, and N is the number of data points. The data residual in general is less than 1.0, which means that the data are fitted within the error bar on the observed (db/dt) data.

To ensure the tTEM system is stable over time, test-site measurements are regularly carried out, typically a couple of times in a survey period. The plots in Figure 7 show the two calibration parameters from the test-site calibration from 10 different days recorded over a period of two and a half months. The calibration factor is constant for the LM data and only drifts 1% for HM data. Except for HM days 9 and 10, the time-shift variation is only 0.1 μs. The small jump in the HM time shift from day 8 to days 9 and 10 can properly be explained by a change of the receiver coil and change of the length of the accompanying cable length. Overall, small and fully acceptable variations indicate that the tTEM system is stable over time, and the assumption of a constant transmitter waveform is justified.

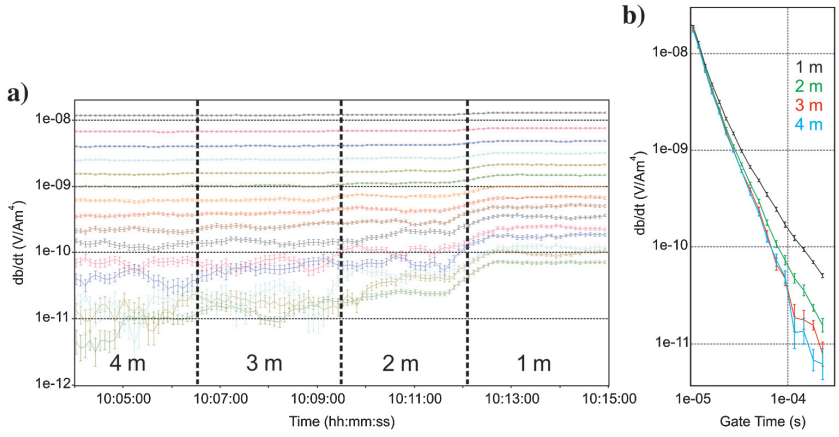

Figure 3. The HM db/dt data with the ATV placed 1, 2, 3, and 4 m from the front of the Tx coil. (a) The single-gate values; each colored line with error bars correspond to a specific gate time. Approximately 2 min of data were recorded at each ATV position. (b) Stacked sounding curves from the center of the four intervals.

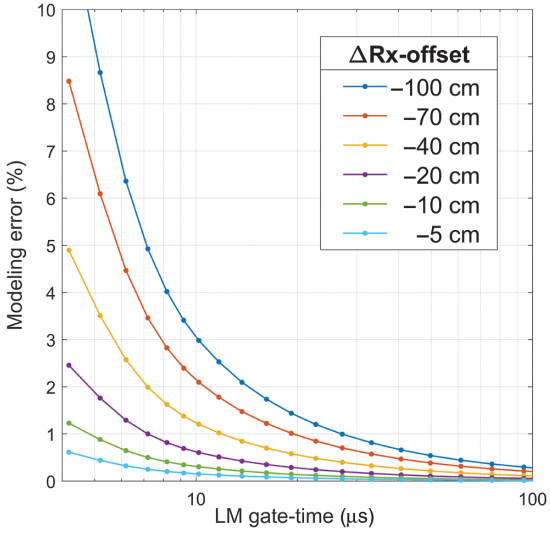

Figure 4. Modeling error for assuming an incorrect Tx-Rx offset. Each curve gives the modeling error for the LM-time gates for at an additional delta offset (see the legend) from the nominal Tx-Rx offset of 11 m.

System validation against borehole

Comparisons of resistivity models from the tTEM survey to existing boreholes with lithologic logs have also been conducted. Figure 8 shows a comparison example from a survey conducted in Vildbjerg, a small town in western Denmark. There are six boreholes (A–F in Figure 8) placed parallel to the tTEM profile, which was recorded approximately 40 m away from the borehole to avoid disturbances from the well infrastructure. In Figure 8, the lithologs are displayed over the resistivity model section. Resistivity models in general show very good agreement with the major lithologic units seen in the boreholes. The top 2–3 m thin, moderately resistive (approximately 55 Ωm) layer (from 155 to 345 m on the *x*-axis) corresponds to the top sandy layer seen in boreholes D and E. This layer diminishes when moving toward boreholes A and B, which is also confirmed by its absence in boreholes B and A. Variations in the thickness of the top clay layer (8–15 m) is characterized by low resistivity (approximately 10–15 Ωm) and underlain by a resistive (approximately 80–200 Ωm) quartz-sand layer. The deep low-resistive layer, starting at approximately 15 m in elevation and seen from 150 to 250 m on the *x*-axis, corresponds to the clay layer, as per the borehole information.

DATA PROCESSING

Signal preprocessing

The noise-suppression techniques used in the tTEM system are similar to those used in most TEM systems. The tTEM transmitter reverses the polarity of alternating pulses, and the EM response is measured in gates with an analog integrator. Following acquisition, the gates are sign corrected, filtered, and stacked (Macnae et al., 1984; Nyboe and Sørensen, 2012). Polarity reversal suppresses low-frequency noise and DC offsets in the receiver electronics. The gates are linearly spaced in logarithmic time to ensure sufficient time resolution in the early gates and optimum S/N at later gates. The periods of the stacks are chosen to cover an integer number of power-line cycles for HM and LM to suppress power-line noise. Further, pulse-repetition frequencies (see Table 1) are chosen so that aliasing of powerful very low frequency (VLF) radio transmitters interferes minimally with the earth response.

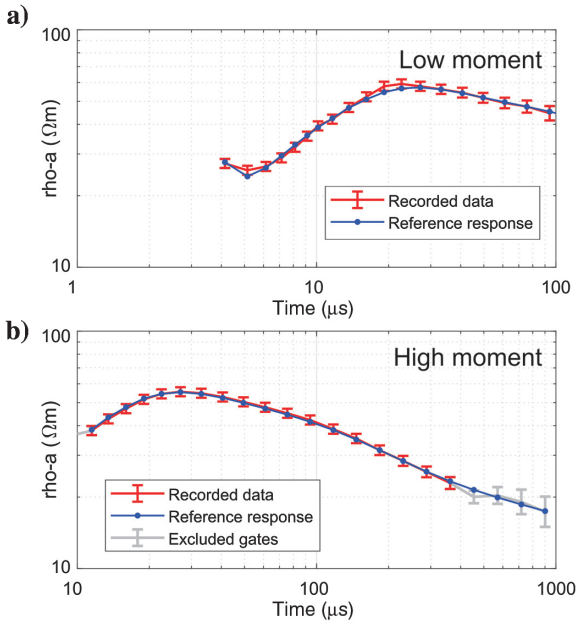

Figure 5. Calibration of the tTEM system. (a) Low moment recorded data (red), and reference response (blue). High moment recorded data (red), and reference response (blue). The nominal error bar size is 2% in the apparent resistivity (rho-a) domain, which corresponds to 3% in voltage data (db/dt) domain. Error bars for late time gates increased based on the STD estimated from data stacking.

When the tTEM system is towed across a rough surface, the receiver coil is exposed to mechanical noise in the form of vibrations and rotations. Rotations of the receiver coil in the earth magnetic field induce noise interfering with the TEM signal. To reduce this noise, the receiver coil is mechanically suspended in tough elastic rubber bands. Experiments based on the receiver coil signal and independent measurements with a 3C gyroscope attached to the receiver coil show that the rotational induced noise is primarily found in the 0–20 Hz frequency range with amplitudes typically being approximately 5–20 $\mu V/m^2$, depending on the velocity of the ATV and the surface roughness.

An example of receiver coil data from the tTEM system is shown in Figure 9 in the form of a spectrogram of HM, gate 17 data. The data are sign corrected before Fourier transforming. The sign-correction flips the spectral location of features in the data; the TEM signal that due to polarity switching initially appeared at fs/2 (where fs is the repetition frequency) is moved to DC, whereas the rotational noise at 0–20 Hz is moved to the fs/2–20 to fs/2 Hz. Each horizontal line in the spectrogram shows the power spectral density from a stack composed of 400 transients. In the first 36 stacks, the tTEM system is stationary and no rotational noise is seen. In the remaining stacks, the system is towed and rotational noise is present at a high frequency. The rotational noise of the sign-corrected data is efficiently suppressed by low-pass filtering as shown in Figure 9b. The low-pass filter is designed with a flat passband from 0 to 15 Hz, 80 dB suppression greater than 75 Hz and the design also includes a notch at fs/2–50 Hz for additional suppression of remaining 50 Hz components. The impulse and frequency response of the low-pass filter are given in Figure 9c and 9d. The data from each gate are low-pass filtered, and the final gate values are obtained by stacking. The gate standard deviation (STD) is calculated from the filtered data. A similar low-pass filter is applied to the low-moment data, with the filter tailored to the low moment repetition frequency.

The motion-induced noise is completely suppressed (>80 dB) due to the fast repetition and the filter. This is contrary to what is known from airborne systems, in which motion-induced noise is a major problem (Allard, 2007).

Data processing and inversion

The processing and inversion of the tTEM data is carried out within the Aarhus Workbench software package. Aarhus Workbench uses the AarhusInv code for modeling and inversion (Auken et al., 2015), capable of handling large TEM data sets with full CPU parallelization using OpenMP in the inversion process. The following is a brief description of the process, and the reader is referred to the referenced papers for all details.

In general, the tTEM processing and inversion scheme follows the processing scheme for SkyTEM data, described by Auken et al. (2009). During the data processing, the coupling from stacked raw data is removed, partly automatically and partly manual. Data from line turns where the ATV gets too close to the Tx are removed as well. Raw stacks are then averaged over a distance, typically approximately 10 m, to create average soundings (stacks). The data points are assigned an uncertainty corresponding to the data STD calculated from the raw transients; however, the minimum uncertainty is limited to 2%.

The inversion of the tTEM data is carried out with spatially constrained 1D smooth models (Viezzoli et al., 2009), forming pseudo 3D model spaces. The inversion algorithm includes modeling of all the key parameters of the system transfer function, such as transmitter waveform, transmitter/receiver timing, low-pass filters, gate widths, and system geometry, which all are essential to obtain accurate data modeling and provide minimally biased inversion results (Christiansen et al., 2011). The inversion result is accompanied by an estimate of DOI (Christiansen and Auken, 2012). Models can be minimized with either an L1-norm (medium blocky), L2-norm (smooth), or a sharp formulation (maximum blocky) (Vignoli et al., 2015).

FIELD EXAMPLE AND APPLICATIONS

Mapping a complex glacial geology

In this section, we show a mapping example to demonstrate the capability/resolution of the tTEM system. The small survey area (Figure 10a) consists of 60 line kilometers of tTEM data covering 1.6 km^2 with line spacing of 25 m, resulting in a total of approximately 6000 single resistivity models. It took two days to collect the data. The survey area is located in the mideast part of Jutland in Denmark, close to the town Gedved, where the area is dominated by glacial deposits on top of tertiary clays. Three mean-resistivity depth slices (shown in Figure 10b and 10c) are created by averaging resistivity over a depth range. From these images, it is clear that the geologic heterogeneity is large with abrupt changes in the geologic layering. Typical resistivities for the sediments are clay-tills (20–40 Ωm), sand/gravel deposits (approximately >50 Ωm), and tertiary clays (approximately <20 Ωm).

The resistivity cross section in Figure 11 again reveals high-resolution geologic/resistivity structures in the target depth interval of 0–50 m. Overall, this tTEM survey and the resulting 3D-resistivity model forms an excellent base for compiling a detailed 3D geologic and/or hydrologic model of the area.

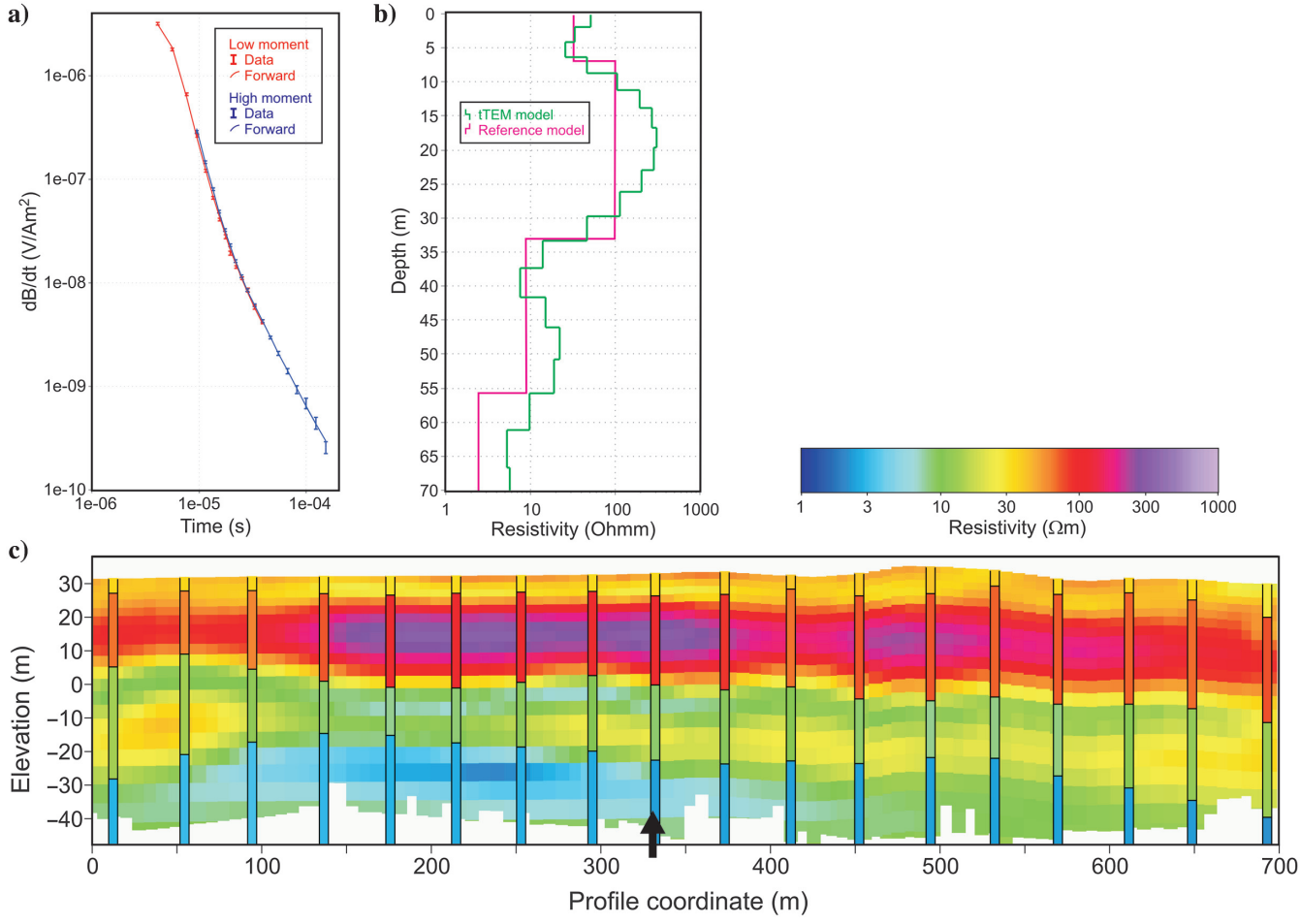

Figure 6. (a) Observed sounding data (low and high moment) and corresponding fit to the forward data. (b) Inverted resistivity model of sounding shown in (a), together with the reference model, (c) vertical resistivity columns are the test-site reference models and background continuous resistivity section is a smooth model inversion of the tTEM data.

Applications

Apart from the above example, we have also successfully used the tTEM system for various other purposes, e.g., mapping construction materials, investigating contaminated sites, mapping the shallow geology for nitrate (N) retention, investigating the geologic setting at artificial recharge sites and, of course, detailed geologic input for hydrogeologic modeling.

Construction materials (sand, gravel, or chalk) underlain by a low-resistivity formation, such as clay, peat or till, are likewise a suitable target to map because the depth to the clay or till can easily be determined with the method. Given the high sensitivity of the TEM method toward the clay layers, it would also be efficient at estimating the thickness of the overburden, making the tTEM system an important tool in the excavation strategy.

Artificial recharge sites play an important role in the sustainable management of groundwater resources. Identifying favorable recharge sites requires an understanding of aquifer systems and their connectivity. In this regard, the tTEM system can be used to provide the image of subsurface structures. For the above purpose, we have successfully conducted tTEM surveys in the fields of the Tulare Irrigation District, an arid region in the California Central Valley, USA.

In many parts of the world, potable groundwater is under stress due to saltwater intrusion. Fresh and saline water are characterized by large resistivity contrasts, making the tTEM system highly suitable in many cases for assessing drinking water quality with respect to saltwater intrusion.

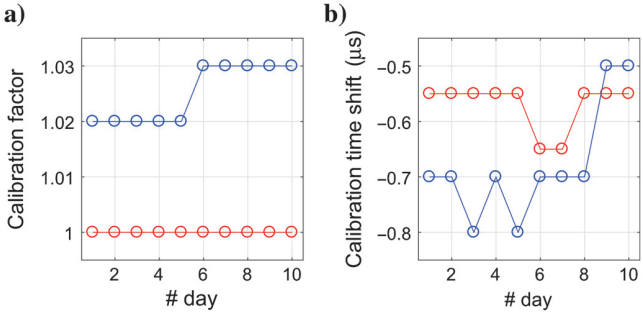

Figure 7. Calibration parameters from 10 different test-site measurements/calibrations, recorded over a period of two and a half months. (a) The calibration factor. (b) The time shift. Red: low moment, and blue: high moment.

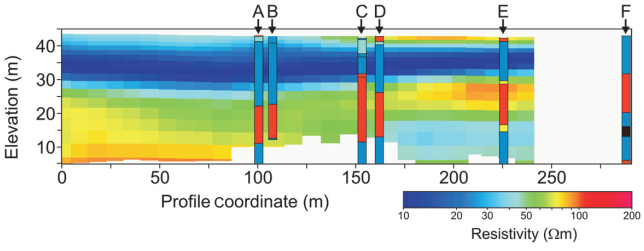

Figure. 8 Resistivity section with lithologs of boreholes from Vildbjerg, Denmark. Borehole lithology: red, sand; blue, clay; light-blue, clay-till; and yellow, silt. Models below the DOI are blanked out (white). The boreholes are offset approximately 40 m from the tTEM line.

In Denmark, increased agricultural productivity has led to the risk of elevated nitrate concentration in surface water and groundwater. To effectively manage and regulate agricultural nitrate use, high-resolution nitrate retention maps are required. The high-resolution mapping capability of tTEM system can provide detailed understating of the hydrogeologic settings, which can improve the prediction of nitrate transport in the open landscape at the field scale. In an ongoing project, we have used tTEM in a few selected agricultural catchments to map the geology in detail as the input to hydrogeologic models.

Another application related to nutrients is the mapping the geologic settings around polluted sites, such as landfills or closed/active point source contaminants. Leachate or pesticides need permeable layers to flow into aquifers. By applying tTEM in an early phase of the investigation of a polluted site, one can track permeable sand/gravel layers and obtain a much better and cost-effective risk assessment compared with just drilling a larger number of boreholes.

As seen in the case study, the system is effective in describing geologic structures due to glacial processes, but it can also be used in other complex geologic settings, such as coastal settings, deltas, estuaries, and fluvial environments. Recently, the system was used for general geologic mapping in the Mississippi Delta, USA. The purpose was to map the complex distribution of sand and clay layers along a meander of the Little Tallahatchie River to support the groundwater modeling.

FURTHER DEVELOPMENTS

The tTEM system in its current version is the result of almost three years of development of the instrumentation and the carrier platform. Our current research focuses on the following implementations: (1) development of more sophisticated signal processing,

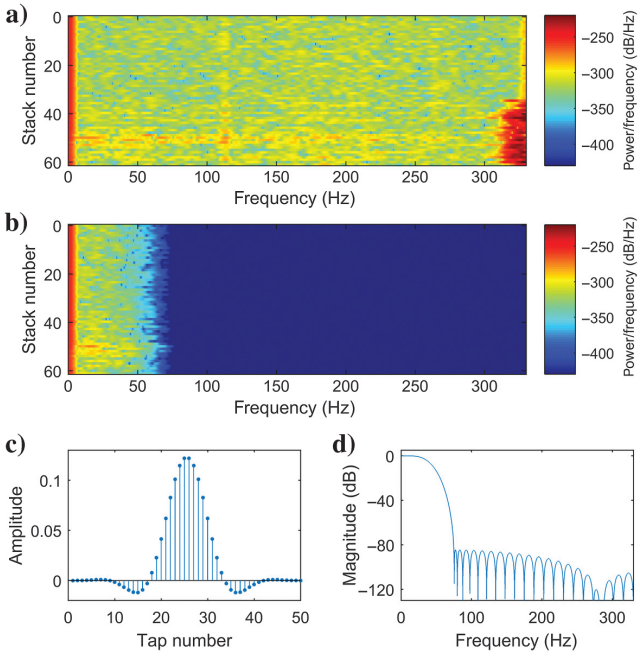

Figure 9. (a) Spectrogram of sign-corrected HM gate 17 (28 µs) data from 60 stacks. (b) Spectrogram after filtering of rotational noise. (c) Impulse response of the designed low-pass filter. (d) Frequency response of low-pass filter.

(2) increasing the resolution of the top meter of the subsurface, and (3) adding wheels to the carrier platform.

Regarding the first development, analysis has shown that the major noise contribution is not vibration-induced noise but amplifier noise and radio-transmitter noise in the 20 kHz range. Amplifier noise can only be suppressed by increasing the area amplification of the receiver coil. However, adding more turns to the coil also lowers the bandwidth, which is not desirable. We are working with different designs, which will maintain a bandwidth of the coil of approximately 600 kHz, while increasing the area by a factor of four from 5 to 20 m^2.The radio-transmitter noise can be suppressed by tapered gating (Macnae et al., 1984); however, our design with analog gating precludes this approach. The workaround is to measure 50–100 gates and then form new tapered gates during processing. This is also ongoing research.

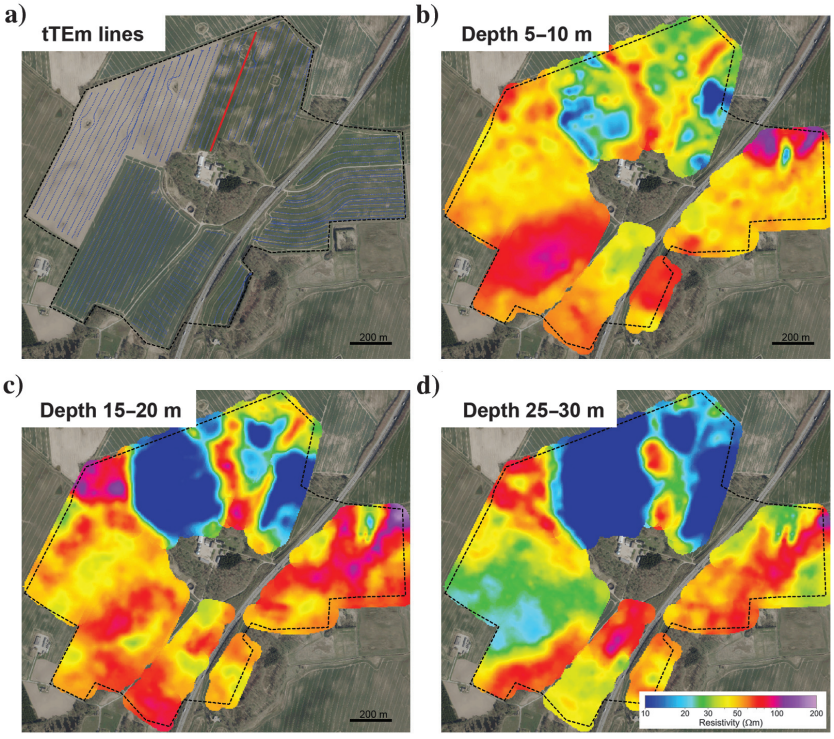

Figure 10. Gedved tTEM survey (dashed polygon). (a) Survey lines (blue dots) and cross-section location (red line), (b) mean resistivity map depth 5–10 m, (c) mean resistivity map depth 15–20 m, and (d) mean resistivity map depth 25–30 m. Resistivity color scale is the same for all plots.

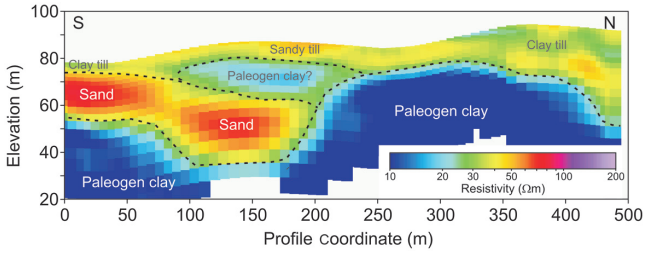

Figure 11. South–north striking cross section. For location, see Figure 10a.

Regarding the second development, resolution of the top 1 m is often desired in farming applications, in which there is a need to map the root zone. Despite the very early first gates and high bandwidth, the system only resolves the average resistivity and not individual layers. At the moment, several experiments are being carried out to study possibilities for increasing the resolution. A potential solution uses a small vertical Tx coil and/or receiver coils.

Regarding the third development, the skids on the sledges wear down after some thousands of kilometers of data collection, and the system cannot be moved from field to field on asphalt. For this reason, we are investigating a wheeled carrier platform or finding another and more robust material for the skids.

CONCLUSION

We have presented a new towed ground-based TEM system, capable of producing high-resolution 3D resistivity models of the subsurface in the depth range of 0–70 m. The system is compact and easy to mobilize and demobilize, and with a mapping speed of up to 20 km/h, it is cost efficient. Being able to map relatively large areas cost effectively in 3D closes a gap in the geophysical toolbox.

We have demonstrated that the tTEM system is a stable system and produces bias-free responses, documented by numerous tests and detailed validation of the system at the Danish TEM test site. With the outlined noise-suppression techniques in signal processing, we have demonstrated that vibration noise is not an issue for the tTEM system, due to the high repetition frequency and efficient filtering.

Careful and detailed processing and modeling of the tTEM data is equally important to obtain high-quality end results. We have outlined our processing and modeling scheme for the tTEM data, which builds on many years of experience with processing and modeling of ground-based TEM and ATEM data.

The field example clearly demonstrates the high-resolution imaging of the subsurface, which can be obtained from tTEM data, providing vital information for compiling detailed 3D geologic/hydrologic models. The further interpretation and integration in a geologic/hydrologic context of some of the larger tTEM surveys already performed will be published later as case studies.

ACKNOWLEDGEMENTS

We would like to thank Kurt Sørensen for numerous fruitful discussion during the development of the system. Also Gert Lauritsen has been of invaluable help in sorting out software problems. Simon Ejlertsen build the first versions of the instruments and Jan Steen Jørgensen kindly help us building the numerous versions of the carrier platform. The development has been funded by Innovation Fund Denmark, project rOpen (Open landscape nitrate retention mapping) and MapField (Field-scale mapping for targeted N-regu-

lation) , WATEC (Aarhus university Centre for water technology) and internal HGG funding.

DATA AND MATERIALS AVAILABILITY

Data associated with this research are confidential and cannot be released.

REFERENCES

Allard, M., 2007, On the origin of the HTEM species: Proceedings of Exploration 07: Fifth Decennial International Conference on Mineral Exploration, 356–373.

Andersen, K. R., N. S. Nyboe, C. Kirkegaard, E. Auken, and A. V. Christiansen, 2015, A system response convolution routine for improved near surface sensitivity in SkyTEM data: 77th Annual International Conference and Exhibition, EAGE, Extended Abstracts, doi: 10.3997/2214-4609.201413874.

Auken, E., T. Boesen, and A. V. Christiansen, 2017, A review of airborne electromagnetic methods with focus on geotechnical and hydrological applications from 2007 to 2017, *in* L. Nielsen, ed., Advances in geophysics: Academic Press Elsevier, 47–93.

Auken, E., A. V. Christiansen, G. Fiandaca, C. Schamper, A. A. Behroozmand, A. Binley, E. Nielsen, F. Effersø, N. B. Christensen, K. I. Sørensen, N. Foged, and G. Vignoli, 2015, An overview of a highly versatile forward and stable inverse algorithm for airborne, ground-based and borehole electromagnetic and electric data: Exploration Geophysics, **46**, 223–235, doi: 10.1071/EG13097.

Auken, E., A. V. Christiansen, J. A. Westergaard, C. Kirkegaard, N. Foged, and A. Viezzoli, 2009, An integrated processing scheme for high-resolution airborne electromagnetic surveys, the SkyTEM system: Exploration Geophysics, **40**, 184–192, doi: 10.1071/EG08128.

Bedrosian, P., C. Schamper, and E. Auken, 2015, A comparison of helicopter-borne electromagnetic systems for hydrogeologic studies: Geophysical Prospecting, **64**, 192–215, doi: 10.1111/1365-2478.12262.

Binley, A., 2015, 11.08 Tools and techniques: Electrical methods, treatise on geophysics: Elsevier.

Bouwer, H., 2002, Artificial recharge of groundwater: Hydrogeology and engineering: Hydrogeology Journal, **10**, 121–142, doi: 10.1007/s10040-001-0182-4.

Christiansen, A., J. B. Pedersen, E. Auken, N. E. Søe, M. K. Holst, and S. M. Kristiansen, 2016, Improved geoarchaeological mapping with electromagnetic induction instruments from dedicated processing and inversion: Remote Sensing, **8**, 1022, doi: 10.3390/rs8121022.

Christiansen, A. V., and E. Auken, 2012, A global measure for depth of investigation: Geophysics, **77**, no. 4, WB171–WB177, doi: 10.1190/geo2011-0393.1.

Christiansen, A. V., E. Auken, and A. Viezzoli, 2011, Quantification of modeling errors in airborne TEM caused by inaccurate system description: Geophysics, **76**, no. 1, F43–F52, doi: 10.1190/1.3511354.

Christensen, N. B., 2014, Sensitivity functions of transient electromagnetic methods: Geophysics, **79**, no. 4, E167–E182, doi: 10.1190/geo2013-0364.1.

Christensen, N. B., and K. I. Sørensen, 2001, Pulled array continuous electrical sounding with an additional inductive source: An experimental design study: Geophysical Prospecting, **49**, 241–254, doi: 10.1046/j.1365-2478.2001.00257.x.

Dahlin, T., C. Bernstone, and M. H. Loke, 2002, A 3-D resistivity investigation of a contaminated site at Lernacken, Sweden: Geophysics, **67**, 1692–1700, doi: 10.1190/1.1527070.

Fitterman, D. V., 2015, 11.10 Tools and techniques: Active-source electromagnetic methods, treatise on geophysics: Elsevier.

Focazio, M. J., 2002, Assessing ground-water vulnerability to contamination: Providing scientifically defensible information for decision makers: U.S. Dept. of the Interior, U.S. Geological Survey 1224.

Foged, N., E. Auken, A. V. Christiansen, and K. I. Sørensen, 2013, Test site calibration and validation of airborne and ground based TEM systems: Geophysics, **78**, no. 2, E95–E106, doi: 10.1190/geo2012-0244.1.

Garman, K. M., and S. F. Purcell, 2004, Applications for capacitively coupled resistivity surveys in Florida: The Leading Edge, **23**, 697–698, doi: 10.1190/1.1776744.

Harris, B. D., P. G. Wilkes, and A. Kepic, 2006, Acquisition of very early time transient electromagnetic data for shallow geotechnical, environmental and hydrogeological applications: Symposium on the Application of Geophysics to Engineering and Environmental Problems, 631–638.

Ibe, K., G. Nwankwor, and S. Onyekuru, 2001, Assessment of ground water vulnerability and its application to the development of protection strategy for the water supply aquifer in Owerri, Southeastern Nigeria: Environmental Monitoring and Assessment, **67**, 323–360, doi: 10.1023/A:1006358030562.

Kirkegaard, C., N. Foged, E. Auken, A. V. Christiansen, and K. I. Sørensen, 2012, On the value of including x-component data in 1D modeling of electromagnetic data from helicopterborne time domain systems in horizontally layered environments: Journal of Applied Geophysics, **84**, 61–69, doi: 10.1016/j.jappgeo.2012.06.006.

Loke, M. H., J. E. Chambers, D. F. Rucker, O. Kuras, and P. B. Wilkinson, 2013, Recent developments in the direct-current geoelectrical imaging method: Journal of Applied Geophysics, **95**, 135–156, doi: 10.1016/j.jappgeo.2013.02.017.

Look, B. G., 2014, Handbook of geotechnical investigation and design tables: CRC Press.

Macnae, J. C., Y. Lamontagne, and G. F. West, 1984, Noise processing techniques for time-domain EM systems: Geophysics, **49**, 934–948, doi: 10.1190/1.1441739.

Maurya, P. K., V. K. Rønde, G. Fiandaca, N. Balbarini, E. Auken, P. L. Bjerg, and A. V. Christiansen, 2017, Detailed landfill leachate plume mapping using 2D and 3D electrical resistivity tomography-with correlation to ionic strength measured in screens: Journal of Applied Geophysics, **138**, 1–8, doi: 10.1016/j.jappgeo.2017.01.019.

Mayer, C. J., and C. T. Somerville, 2000, Land use regulation and new construction: Regional Science and Urban Economics, **30**, 639–662, doi: 10.1016/S0166-0462(00)00055-7.

Møller, I., V. H. Søndergaard, and F. Jørgensen, 2009, Geophysical methods and data administration in Danish groundwater mapping: Geological Survey of Denmark and Greenland Bulletin, **17**, 41–44.

Nyboe, N. S., F. Jørgensen, and K. I. Sørensen, 2010, Integrated inversion of TEM and seismic data facilitated by high penetration depths of a segmented receiver setup: Near Surface Geophysics, **8**, 467–473, doi: 10.3997/1873-0604.2010026.

Nyboe, N. S., and K. I. Sørensen, 2012, Noise reduction in TEM: Presenting a bandwidth- and sensitivity-optimized parallel recording setup and methods for adaptive synchronous detection: Geophysics, **77**, no. 3, E203–E212, doi: 10.1190/geo2011-0247.1.

Saey, T., M. Van Meirvenne, P. De Smedt, B. Stichelbaut, S. Delefortrie, E. Baldwin, and V. Gaffney, 2015, Combining EMI and GPR for non-invasive soil sensing at the Stonehenge World Heritage site: The reconstruction of a WW1 practice trench: European Journal of Soil Science, **66**, 166–178, doi: 10.1111/ejss.12177.

Schamper, C., E. Auken, and K. I. Sørensen, 2014a, Coil response inversion for very early time modeling of helicopter-borne time-domain electromagnetic data and mapping of near-surface geological layers: Geophysical Prospecting, **62**, 658–674, doi: 10.1111/1365-2478.12104.

Schamper, C., F. Jørgensen, E. Auken, and F. Effersø, 2014b, Assessment of near-surface mapping capabilities by airborne transient electromagnetic data: An extensive comparison to conventional borehole data: Geophysics, **79**, no. 4, B187–B199, doi: 10.1190/geo2013-0256.1.

Sophocleous, M., 2002, Interactions between groundwater and surface water: The state of the science: Hydrogeology Journal, **10**, 52–67, doi: 10.1007/s10040-001-0170-8.

Sørensen, K. I., 1996, Pulled array continuous electrical profiling: First Break, **14**, 85–90.

Sørensen, K. I., 1997, The pulled array transient electromagnetic method: Proceedings of the 3rd Meeting of the Environmental and Engineering Geophysical Society, European Section, 135–138.

Sørensen, K. I., and E. Auken, 2004, SkyTEM: A new high-resolution helicopter transient electromagnetic system: Exploration Geophysics, **35**, 191–199.

Viezzoli, A., E. Auken, and T. Munday, 2009, Spatially constrained inversion for quasi 3D modeling of airborne electromagnetic data: An application for environmental assessment in the lower Murray region of South Australia: Exploration Geophysics, **40**, 173–183, doi: 10.1071/EG08027.

Vignoli, G., G. Fiandaca, A. V. Christiansen, C. Kirkegaard, and E. Auken, 2015, Sharp spatially constrained inversion with applications to transient electromagnetic data: Geophysical Prospecting, **63**, 243–255, doi: 10.1111/1365-2478.12185.